View metadata, citation and similar papers at core.ac.uk

brought to you by CORE

provided by ScholarWorks@UMass Amherst

University of Massachusetts Amherst
ScholarWorks@UMass Amherst

Astronomy Department Faculty Publication Series | Astronomy

1997

Globular cluster evolution in M87 and fundamental plane ellipticals

C Murali

MD Weinberg

Follow this and additional works at: https://scholarworks.umass.edu/astro_faculty_pubs


Part of the Astrophysics and Astronomy Commons

Recommended Citation

Murali, C and Weinberg, MD, "Globular cluster evolution in M87 and fundamental plane ellipticals" (1997). *MONTHLY NOTICES OF THE ROYAL ASTRONOMICAL SOCIETY*. 76.
10.1093/mnras/288.3.767

This Article is brought to you for free and open access by the Astronomy at ScholarWorks@UMass Amherst. It has been accepted for inclusion in Astronomy Department Faculty Publication Series by an authorized administrator of ScholarWorks@UMass Amherst. For more information, please contact scholarworks@library.umass.edu.

Mon. Not. R. Astron. Soc. **000**, 000–000 (0000) Printed 5 February 2008 (MN LATEX style file v1.3)

Globular Cluster Evolution in M87 and Fundamental Plane Ellipticals

Chigurupati Murali and Martin D. Weinberg⋆
Department of Physics and Astronomy, University of Massachusetts, Amherst, MA 01003-4525, USA

5 February 2008

arXiv:astro-ph/9602058v2 13 Feb 1996

ABSTRACT

The globular cluster population in M87 has decreased measurably through dynamical evolution caused by relaxation, binary heating and time-dependent tidal perturbation. For fundamental plane ellipticals in general, cluster populations evolve more rapidly in smaller galaxies because of the higher mass density. A simple evolutionary model reproduces the observed trend in specific frequency with luminosity for an initially constant relationship.

Fits of theoretically evolved populations to M87 cluster data from McLaughlin et al. (1994) show the following: 1) dynamical effects drive evolution in the initial mass and space distributions and can account for the large core in the spatial profile as well as producing radial-dependence in the mass spectrum; 2) evolution reduces S_N by 50% within 16 kpc and 35% within 50 kpc, implying that S_N was initially 26 in this region. We estimate that 15% of the 'missing' clusters lie below the detection threshold with mass less than $10^5 M_\odot$.

Key words: globular clusters: general – galaxies: individual (M87) – galaxies: star clusters

1 INTRODUCTION

Observations of some giant elliptical galaxies reveal globular cluster systems which appear more extended than the host (Harris 1991). A particularly well-documented example belongs to M87 with a core radius of 7 arc sec and a cluster system with a core radius of 1 arc min (McLaughlin 1995). However, because a cluster population evolves dynamically due to both internal and external processes, the currently observed population almost certainly differs from the primordial one, complicating the interpretation.

Researchers have attempted to explain the extended core of the M87 cluster distribution as the evolved remnant of an initial profile which more closely resembled the light. However, neither dynamical friction nor shocking by a compact nucleus can fully account for this feature. Lauer & Kormendy (1986) found that a dynamical friction induced inflow can broaden an initially peaked spatial distribution but not at the observed scales. Ostriker, Binney & Saha (1989, hereafter OBS) subsequently determined that nuclear tidal disruption is viable only if clusters formed exclusively on box orbits.

Another potential mechanism is cluster evaporation through dynamical evolution. Recent work in this area demonstrates that evaporative mass loss driven by relaxation and heating due to a time-varying tidal field can lead to strong evolution of the Milky Way cluster population in a Hubble time (Weinberg 1994, Murali & Weinberg 1996, hereafter MW). In this paper, we examine these influences on cluster evolution in the dense inner regions of M87 and find that they produce the observed flattened profile from a peaked initial distribution over a wide range of initial conditions. Direct estimates of initial conditions using dynamically evolved parametric models of the spatial distribution and cluster mass function indicate that roughly 35% of the initial population dissolves or evolves below the detection threshold leaving the large core as a result. Furthermore, the decay in the size of the cluster population corresponds to a decrease in the specific frequency of globular clusters, S_N, which denotes the number of clusters per unit galaxian luminosity with L measured in units of $M_v = -15$.

The high values of S_N found in giant ellipticals have become a key point in galaxy formation arguments and suggest, for example, that the cluster system formed along with M87 (e.g. Harris 1991; van den Bergh 1995). Here we show that cluster systems decay more rapidly in less luminous fundamental plane ellipticals; this leaves larger values of S_N in luminous galaxies at the present epoch even if all ellipticals begin with equal S_N. Our results thus provide at least a partial explanation for the observed trend of S_N with L.

⋆ Alfred P. Sloan Foundation Fellow.

The plan of the paper is as follows. We summarize our choices for the cluster population and the mass model for M87 in §2. The assumptions and method for dynamically evolving the population is presented in §3. The main results, the statistical comparison of the observed clusters to the theoretical models, is presented in §4. This includes an exploration of the evolutionary trends, best fit spatial profiles and mass functions, and an inference of the primordial population. In §5, we discuss the discuss the importance of the fundamental plane properties on the observed relation between specific frequency and luminosity A summary is given in §6.

2 CLUSTER POPULATION

We assume that the cluster population formed in an initial burst approximately 11 Gyr ago. Stellar evolution dominated cluster evolution for the first Gyr for a Salpeter IMF ($\beta = 2.35$) with $m_l = 0.1\,\mathrm{M}_\odot$, corresponding to the main sequence lifetime of $2\,\mathrm{M}_\odot$ A-star. Our zero-age population represents the epoch when, approximately 10 Gyr ago, relaxation, external heating and core collapse heating began to drive cluster evolution.

The fiducial calculations represent zero-age clusters as $W_0 = 5$ King models. Comparison calculations using $W_0 = 7$ clusters show nearly identical evolution over the long time scales of interest, in agreement with the results of MW where overall evaporation times were found to depend weakly on concentration in the range $5 \leq W_0 \leq 7$. We expect similar trends in evolution for $W_0 = 3$ clusters (c.f. MW), except in high mass, low-eccentricity cases where tidal heating leads to rapid disruption. These clusters enhance the destruction rate described below, but constitute a very small fraction of expected initial populations.

Each cluster is tidally limited on its orbit in the host. While initial cluster densities may differ from the mean density required by perigalactic tidal limitation, subsequent evolution during the first Gyr leads rapidly to tidal truncation or disruption. The limiting or *tidal* radius R_T is uniquely determined by the cluster mass and orbit. Table 1 summarizes the choice of parameters for individual clusters.

To represent the cluster mass distribution, $\nu(M, r)$, we use pure power laws (e.g. Harris & Pudritz 1994), power laws whose exponents have a linear dependence on radius, and a Gaussian magnitude distribution (e.g. McLaughlin, Harris & Hanes 1994, MHH). Power law mass distributions have been proposed on physical grounds by Harris & Pudritz (1994) while the Gaussian is commonly used as a convenient fitting function for the observed cluster luminosity function. To represent the spatial distribution of the cluster population in the primary, we use power law densities with and without a core derived from isotropic distribution functions, $f(E)$. Orbital isotropy is assumed due to lack of observational constraint.

Adopted models are given by joint distributions $\nu(M, r) \times f(E)$ and are summarized in Table 2. The Model 1 and Model 2 families use power law mass and Gaussian magnitude distributions respectively. Within each family, successive models have additional parameters to explore varying core sizes and radial dependence of the mass spectral index. Detailed derivation of models from the underlying distribution function is given in Appendix A.

Finally, we represent the potential of M87 as a singular isothermal sphere, with rotation velocity $v_0 = 606\,\mathrm{km\,s^{-1}}$ (e.g. OBS), velocity dispersion $\sigma = 350\,\mathrm{km\,s^{-1}}$, and assume a distance of 16 Mpc (van der Marel 1992). This defines a length scale of 77.6 pc per second of arc. Further discussion of potential and distance scale is given in Appendix B.

3 CLUSTER EVOLUTION

Competition between internal relaxation and heating due to external forcing may dramatically affect a cluster's evolutionary time scale and survival history. In addition to impulsive heating of a cluster halo—in a gravitational bulge shock, for example—resonances between the cluster's own orbital motion and internal stellar trajectories may heat cluster stars beyond the limit set by adiabatic invariance (Weinberg 1994). For tidally-limited clusters resonant heating on low-eccentricity orbits and tidal limitation on high-eccentricity orbits drive rapid cluster evolution and evaporation (see MW for details). The strength of these effects motivates this study.

The evolution of individual clusters includes two-body relaxation in the one-dimensional Fokker-Planck approximation (e.g. Cohn 1979), external heating due to the time-varying tidal field (MW), and a phenomenological binary heating term (e.g. Lee et al. 1991).

We take advantage of the scale-free galaxian profile by fixing orbital energy E of all clusters, choosing an initial grid of tidally-limited clusters in $\kappa = J/J_{max}(E)$ and mass, and computing the evolution to complete evaporation. The quantity $J_{max}(E)$ denotes the maximum angular momentum of an orbit with energy E. This grid may then be scaled to all desired orbital energies. The time evolution of the space density for the entire population is then constructed by determining the phase space distribution at the desired time using the evolutionary calculations and projecting appropriately.

Although we specifically consider M87, the results apply to any elliptical with similar profile. For example, we can scale evolution to any fundamental plane elliptical. Because the period decreases with mass, the same initial population will be more evolved for smaller mass primaries (see §5 for more discussion).

4 RESULTS

4.1 Evolution of the core

An initially peaked cluster distribution develops a flattened core through dynamical evolution of individual clusters, as shown in Figure 1. In the dense regions of the inner galaxy, rapid mass loss due to relaxation and tidal heating can cause complete evaporation of a cluster or drive it below the observational limit. Rapid relaxation results from the high densities imposed by tidal limitation while tidal heating strongly enhances evaporation rates on low-eccentricity orbits. The resulting profiles are similar to the profile derived in McLaughlin (1995).

The overall shape of the evolving profile depends on

Table 1. Cluster Initial Conditions

Structural parameters		Fiducial value
M	total mass	$10^5 \leq M_c \leq 5 \times 10^6 M_\odot$
W_0	King concentration parameter	$W_0 = 5, 7$
R_T	cluster limiting radius	tidal limitation
Mass spectral parameters		
β	mass spectral index: $N(m) \propto m^{-\beta}$	$\beta = 2.35$ (Salpeter)
m_l	lower mass limit	$m_l = 0.1$
m_u	upper mass limit	$m_u = 2.0$
Orbital parameters		
E	orbital energy	isotropic orbit
κ	relative ang. mom.: $J/J_{max}(E)$	distribution

Table 2. Population models

Designation	$\rho(r)$	$\nu(M)$	Parameters
Model 1a	$\rho_0 r^{-\eta}$	$M^{-\alpha}$	η, α
Model 1b	$\rho_0 r^{-\eta}$	$M^{-(\alpha+Kr)}$	η, α, K
Model 1c	$\rho_0 (r_c^2 + r^2)^{-\eta/2}$	$M^{-\alpha}$	η, r_c, α
Model 1d	$\rho_0 (r_c^2 + r^2)^{-\eta/2}$	$M^{-(\alpha+Kr)}$	η, r_c, α, K
Model 2a	$\rho_0 r^{-\eta}$	$e^{-(V-V_0)^2/2\sigma_V^2} \cdot dV/dM$	η, V_0, σ_V
Model 2b	$\rho_0 (r_c^2 + r^2)^{-\eta/2}$	$e^{-(V-V_0)^2/2\sigma_V^2} \cdot dV/dM$	η, r_c, V_0, σ_V

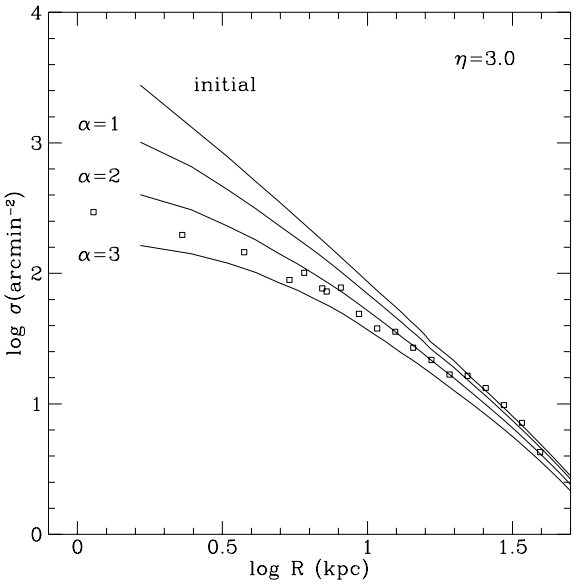

Figure 1. Surface density inferred from observations (open squares) compared to Model 1a for indicated values of mass spectral index α and initial r^{-3} ($\eta = 3$) profiles (solid curves). Rapid evolutionary rates of low mass clusters produce flatter cores for larger α.

both the initial mass and space distribution of the clusters. Consider the following limits. For a fixed spatial profile, a distribution rich in low mass clusters evolves rapidly due to short evaporation times while for a fixed mass distribution, a sharply peaked spatial profile develops a smaller core than a shallow profile. Taken together, the two trends produce a correlation between the inferred initial mass distribution and density profile: a large population of low mass clusters can rapidly flatten a steep initial profile while, conversely, a large population of high mass clusters allows a flatter initial profile to evolve slowly to the same final shape. Observations of the cluster mass distribution will distinguish between the different initial conditions.

4.2 Estimates of initial conditions

The evolved cluster populations described in §3 are compared to observed cluster data† using a maximum likelihood estimator which combines model and background surface densities with incompleteness measurements. The background surface density is taken to be 6.33 per arcmin^2 with a uniform luminosity function (MHH). Point sources lie in the region $1.21' \leq R \leq 7'$ (the field edge), centered on M87, with apparent limiting magnitude $V = 24$. We use a mass-to-light ratio $(M/L)_V = 2$ to convert luminosity to mass. Note that larger M/L will shift the population to higher mass, implying less evolution, while smaller M/L will have the opposite effect. For $R < 1.21'$, the authors provide 3 binned points (McLaughlin 1995). A joint χ^2-likelihood estimator is used to include all data points. Details of the estimation procedure are provided in Appendix C.

We fit both dynamically evolved distributions and unevolved distributions based on the models presented in Table 2. In the case of dynamically evolved models, the quoted values represent initial conditions (labeled by 'initial'). In the case of unevolved models, the quoted values represent the best fit parameters at the present epoch (labeled by

† The data have been kindly supplied by McLaughlin & Harris (1995)

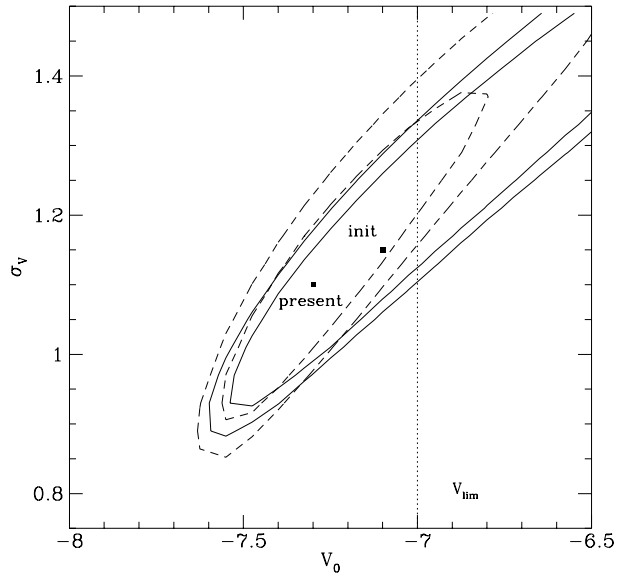

Figure 2. 95% and 99% confidences for marginal density in V_0 and σ_V for present (dashed) and initial (solid) Model 2a fits. Points indicate best-fit values for present and initial models. The magnitude limit of the data is indicated as the vertical line.

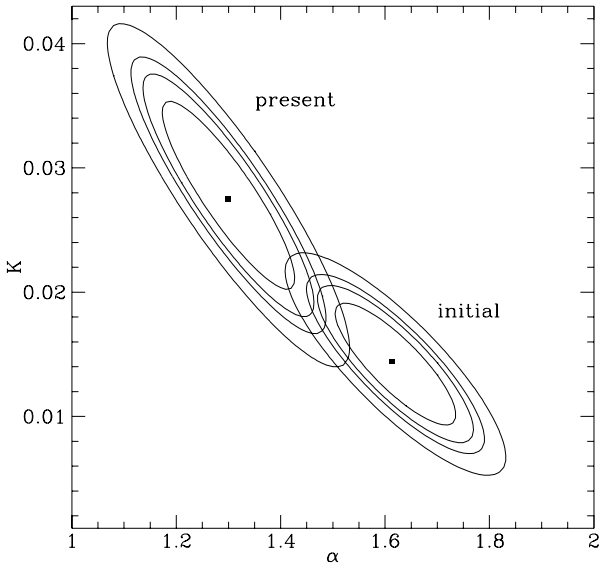

Figure 3. 75%, 90%, 95%, and 99% confidences for marginal density in α and K for present epoch and initial Model 1d fits. Points mark best-fit values. The initial spectral index shows mild radial dependence increasing from a central value of 1.61 to 1.97 at 30 kpc in the best-fit case.

'present'). Only models with cores are considered in the present epoch fits because coreless models poorly represent the data.

Tables 3 and 4 present the best estimates and their variances (cf. Table 2). Comparison of present epoch and initial parameter estimates illustrates several expected evolutionary trends. The core of the distribution grows due to the depletion of clusters in the inner regions of the galaxy. The power law index α decreases, while the Gaussian magnitude peak V_0 and slope K of the radially-dependent power law both increase as a result of the selective evaporation of lower mass clusters. The increase in K also indicates that depletion occurs primarily in the inner regions. The following cases show specific features of these trends.

We plot the marginal probability density in V_0 and σ_V for Model 2b in Figure 2. The best estimate for V_0 decreases with time as low mass (and therefore high V) clusters disappear. However, the assumption of identical initial and present epoch values cannot be ruled out since the values of V_0 are only weakly inconsistent (cf. Table 4). The lack of constraint could result from the shallow magnitude limit of the data. Both fits are consistent with distributions which peak below the limiting magnitude of $V = -7$.

Model 1d suggests that there is radial dependence in the mass distribution (Fig. 3). Both present epoch and initial fits are inconsistent with a constant mass spectral index ($K = 0$) and indicate that dynamical evolution has enhanced the radial dependence. In the core region, the present index $\alpha \approx 1.4$. We note that these results conflict with those of MHH and McLaughlin & Pudritz (1996), who find no radial dependence in the mass distribution.

4.3 Comparison of models

The previous section examined the results of trends in the evolution of the cluster population within several model families. Here, we identify the best overall representation among the initial models after 10 Gyr of evolution using a generalized likelihood ratio test (e.g. Martin 1971).

The final column in Table 3 shows that the most general model gives a better estimate in each case, as expected. In particular, Model 1c can be rejected in favor Model 1d, a result which is consistent with the confidence surfaces for the radially-dependent mass spectrum plotted in Figure 3.

Model 2b generalizes Model 2a by introducing arbitrary *initial* core size. A finite core does provide a better estimate but zero core (Model 2a) cannot be rejected. Figure 4 compares the surface density profiles of these two models. The Model 2b fit falls below the observed profile at small radii due to the shallow initial core. However, the binned surface density points have relatively low weight in the full data set. The good fit of Model 2a to the inner data points suggests that a more peaked initial distribution may provide the optimal fit. The use of individual cluster counts in this region should help provide the necessary constraint. The deviation of the present epoch fit from the data further suggests that evolution plays an important role in shaping the profile.

Finally, we compare the most general power law mass function model, Model 1d, with the most general Gaussian magnitude model, Model 2b, by constructing a linear combination of both spaces and searching for the global maximum. The maximum occurs at the best-fit parameters for Model 2b: the Gaussian magnitude distribution describes the data significantly better than any power law mass distribution. As discussed above, the Gaussian may be poorly constrained by

Table 3. Model 1 fits

Epoch	η	σ_η	r_c	σ_{r_c}	α_0	σ_{α_0}	K	σ_K	-log L
Model 1a									
initial	2.76	0.04	-	-	1.95	0.03	-	-	69502.9
Model 1b									
initial	2.66	0.06	-	-	1.68	0.09	0.01	0.004	69501.3
Model 1c									
present	3.09	0.13	7.30	0.79	1.73	0.04	-	-	69500.6
initial	3.03	0.12	5.67	0.94	1.93	0.04	-	-	69499.8
Model 1d									
present	3.06	0.13	7.34	0.81	1.30	0.08	0.028	0.002	69480.9
initial	3.13	0.10	5.70	0.40	1.61	0.10	0.014	0.004	69492.8

Table 4. Model 2 fits

Epoch	η	σ_η	r_c	σ_{r_c}	V_0	σ_{V_0}	σ_V	σ_{σ_V}	-log L
Model 2a									
initial	2.77	0.05	-	-	-7.11	0.17	1.16	0.08	69487.2
Model 2b									
present	3.10	0.13	7.32	0.80	-7.33	0.10	1.08	0.07	69468.7
initial	3.14	0.12	5.14	0.77	-7.07	0.17	1.19	0.08	69485.3

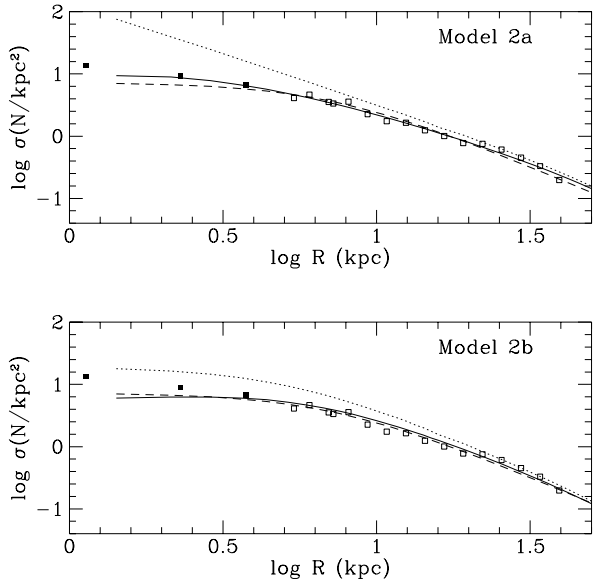

Figure 4. Comparison of surface density profiles of Models 2a and 2b (solid) with binned data. Initial profiles (dotted) and present epoch Model 2b fits (dashed) are also plotted. Both the model with initial core and the present epoch fit deviate from the data in the inner region.

the limiting magnitude of the data. However, examination of the estimated functions shows that the power law is more peaked at low mass than the Gaussian both initially and finally, while the Gaussian has more weight at high mass. Thes differences in shape also lead to the statistical preference of the Gaussian luminosity function over the spatially constant power law and its radially-dependent generalization.

Table 5. Evolved model comparisons

test	$-2\ln\lambda^\flat$	$\nu^\sharp$	accept	reject	confidence
1c–1d	14.0	4		√	99%
2a–2b	3.8	4	√		60%
1d–2b	15.0	7		√	96%

$^\flat -2\ln\lambda$ is likelihood ratio
$^\sharp\nu$ is number of degrees of freedom

Table 5 summarizes the conclusions of the tests comparing the initial conditions and lists the likelihood ratios and confidence values. In the first two cases, the likelihood ratios follow directly from Tables 3 and 4. In summary, we find that the initial Gaussian magnitude distribution best describes the data, but that we cannot distinguish between singular density profiles and densities with core. Both conclusions may result from insufficient data.

4.4 Evolution of the initial population

From the derived initial conditions, we plot the projected cumulative distribution of clusters initially within 50 kpc or $6.5R_e$ (Figure 5). The initial population in this region is about 7250 for Model 2a, a factor of 1.6 larger than the presently observed population of 4500. For Model 2b, the initial population size is smaller, but still in excess of 6000. Evolved clusters will also be found at masses below the observational limit. Within 16 kpc, about 500 evolved clusters are expected in the range $24 > V > 24.5$ ($10^5 > M > 7\times10^4 M_\odot$). All other clusters in this region initially in this mass range will have evaporated.

This implies that the specific frequency, S_N, evolves with time. Using the ratio of final to initial surface densities from the models, we derive the run in initial specific frequency at radius R, $S_N(R)$ (Figure 6). As expected, depletion in the inner regions dominates; however, $\sim 10\%$ change

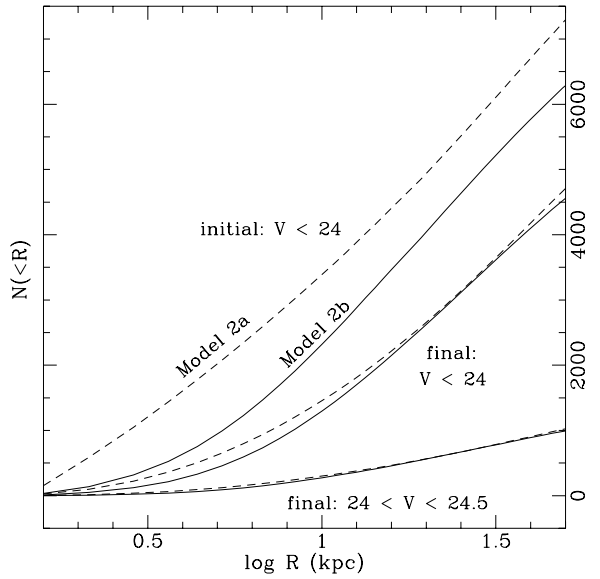

Figure 5. Estimated cumulative distribution of clusters for projected radius $R < 50\,\mathrm{kpc}$ ($6.5R_e$). Initial distributions for Model 2a (dashed) and Model 2b (solid) are shown for $V < 24$ (upper pair). Final distributions are shown for $V < 24$ (middle pair) and for $24 > V > 24.5$ (bottom pair). Clusters with $24 > V > 24.5$ began with $V < 24$. Approximately 50% of the initial clusters vanish within (16 kpc) $2R_e$ and 35% within $6.5R_e$ for Model 2a.

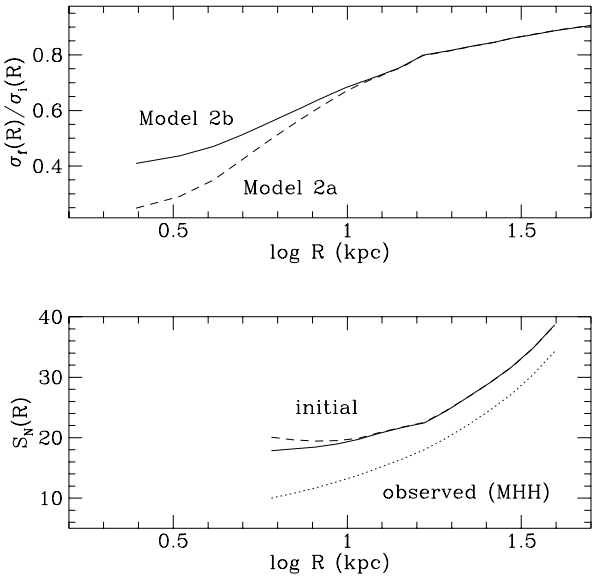

Figure 6. The ratio of final to initial surface density (top) in Models 2a (dashed) and 2b (solid) and the run in initial specific frequency at R ($S_N(R)$) for each model (bottom) derived from the observed values given by MHH (dotted). Evolution reduces S_N by 35% in Model 2a.

in $S_N(R)$ occurs even out to 50 kpc due to the rapid evolution of low-mass clusters.

Model 2a in Figure 5 shows a 35% change in total S_N within 50 kpc due to depletion. The observed total value $S_N \approx 17$ in this region (MHH) implies an initial value of 26.5. Thus even the enormous observed value of S_N has diminished significantly due to evolution (this neglects the intrinsic evolution in galaxy luminosity due to stellar evolution). The time evolution of the total S_N is shown directly in Figure 7. The decay of the cluster population is approximately exponential in time with e-folding times of 20 Gyr and 40 Gyr for measurements within 16 and 50 kpc, respectively.

Our comparison applies to clusters in specified mass and radial ranges in a galaxy. Quoted specific frequency values are extrapolated over unobserved ranges from data taken within such limits. In the case of M87, MHH find $S_N = 17.7$ directly from the observations, while extrapolation yields a total $S_N = 14.4$ for the whole galaxy. Their extrapolation of the luminosity function over all magnitudes yields a total correction of 2.2 to cluster counts in the observed magnitude range. For $R < 42\,\mathrm{kpc}$, using this correction they estimate a total ~ 9400 clusters (3729 observed in galaxy+cD envelope, 500 in core, $\times 2.2$) which is 70% of the total number of clusters estimated over all radii. The estimated initial distribution has a larger correction because it is weighted more heavily to low mass (c.f. §4.2). Since most of these clusters completely evaporate, this implies even greater evolution in specific frequency than derived here.

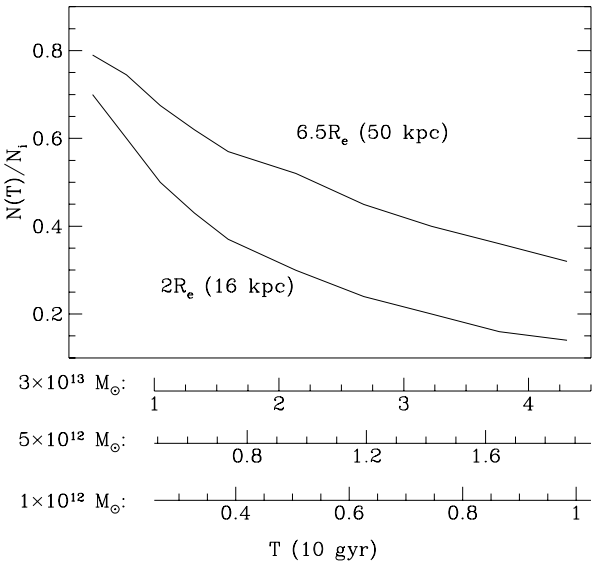

Figure 7. The fraction of clusters remaining within the indicated projected radius as a function of time. Abscissae indicate time units which correspond to fundamental plane scaling for galaxies with indicated masses. Top axis gives M87 scaling (other axes will be discussed in the next section). Initial S_N is ≈ 21 measured within 16 kpc and 26.5 measured within 50 kpc and decays with the cluster population.

5 DISCUSSION

Our conclusions ignore the possibility that recent merger and accretion events have have strongly contaminated the initial cluster population. Merging of gas-rich galaxies is expected to produce clusters with strong central concentration (Zepf & Ashman 1993; Mihos & Hernquist 1994), but the large core of the distribution itself argues against any recent merger which has produced significant numbers of young clusters. Thus either cluster-producing mergers in M87 have occurred long in the past or not at all.

The recent addition of clusters through satellite accretion is also unlikely to account for a significant fraction of the observed population. For example, accretion of Milky Way-type spirals can only account for about 25% of the observed population, assuming that the $4L_*$ luminosity of M87 ($R < 40\,\mathrm{kpc}$) comes entirely from satellites (Lauer 1988). Assuming that material is stripped when the mean density of the primary exceeds that in the satellite, accretion will deposit clusters in regions of mean density similar to that in the original environment of the accreted galaxy. The clusters, then, will remain roughly tidally truncated. Their new orbits depend on the orbit of the dissolving satellite, but otherwise evolution should be similar and the accreted population may appear coeval regardless of the time of accretion.

The high specific frequency of globular clusters in M87 appears to indicate the exceptional conditions governing the formation and evolution of cD galaxies relative to other ellipticals. The observation that specific frequency increases with galaxy luminosity suggests that galaxy formation was not an intrinsically hierarchical and homologous process (e.g. Santiago & Djorgovski 1993).

However, the current results indicate that density differences between galaxies will lead to differences in the evolution of intrinsic cluster populations. Since M87 lies approximately on the fundamental plane for elliptical galaxies, we can investigate differences in environment-driven cluster evolution by scaling our results to other ellipticals. We assume that the initial profile of the cluster population derived above, when scaled homologously, describes the initial population in any elliptical. The dynamical time scale for a tidally truncated cluster with constant mass and spatial profile is then determined by the mean density of the galaxy: $\tau \sim M^{-1/2}R^{3/2}$. This yields $\tau \sim M^{\beta}$, where $\beta = 0.4$ for the fundamental plane scaling given in Faber et al. (1987), $\beta = 0.26$ for the Djorgovski & Davis (1987) results, and $\beta = 0.6$ for a more recent set of parameters from Faber (1995; see also Pahre et al. 1995). This relation implies that clusters evolve and are depleted more rapidly in smaller, low luminosity ellipticals than in massive, high luminosity ellipticals.

To demonstrate the importance of this effect, we combine the approximate exponential decay rate of the cluster population found in §4.4 with this scaling relation. This gives an expression for the number of clusters remaining in an initially coeval population belonging to a galaxy of luminosity L at time T:

$$N_{cl}(L,T) = N_0(L)e^{-T/\tau_0(M_{M87}/M)^{\beta}} = N_0 e^{-T/\tau_0(L_{M87}/L)^{1.24\beta}}, \quad (1)$$

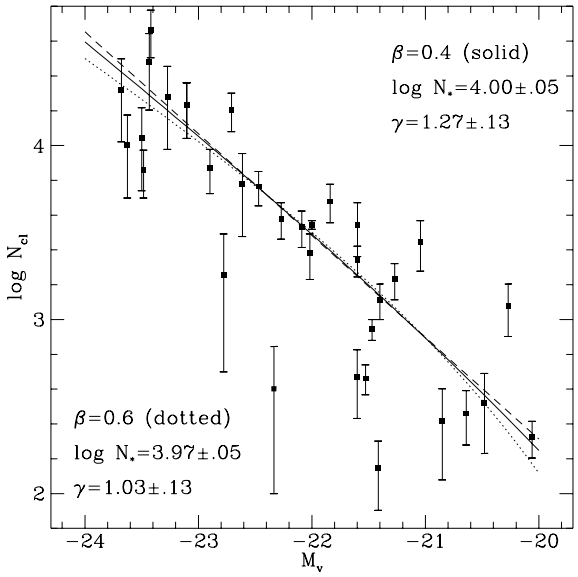

Figure 8. Evolved population size as a function of galaxy luminosity compared to data from Harris (1996) for fundamental plane parameter $\beta = 0.4$ (solid) and $\beta = 0.65$ (dotted) . The present-day, unevolved fit (dashed) has $\log N_* = 3.89 \pm .05, \gamma = 1.46 \pm .13$. For $\beta = 0.65$, the initial value of γ is consistent with specific frequency which is independent of luminosity

where $\tau_0 \approx 40\,\mathrm{Gyr}$ for M87, $N_0(L)$ is the initial distribution of cluster population sizes as a function of galaxy luminosity and $M/L \sim L^{1.24}$ throughout.

Using a power-law distribution $N_0(L) = N_*(L/L_{M87})^{\gamma}$, we compare the model curve $N_{cl}(L,T)$ to an observed sample of cluster populations in galaxies (Harris 1996). The resulting models show qualitative agreement with the data (Figure 8), falling off at low luminosity more rapidly with increasing β due to the more rapid rate of evolution. From this we conclude that the observed discrepancies in specific frequency which correlate with galaxy luminosity were smaller in the past. This is reflected in the smaller exponent γ in $N_{cl} \propto L^{\gamma}$ predicted initially compared to the present-day estimate.

To conclude, we suggest that cluster evolution may account at least in part for the specific frequency problem. Because clusters evolve more rapidly in dense environments and because ellipticals are typically denser at low luminosity that at high luminosity, cluster populations diminish more rapidly in low luminosity galaxies. Specific frequencies will therefore correlate more strongly with luminosity at later times.

6 SUMMARY

We have investigated the evolution of the M87 globular cluster system. The results of this study have enabled us to examine the broader question of population evolution in fundamental plane elliptical galaxies. Our main conclusions follow:

(i) The loss of globular clusters through relaxation and

tidally-induced evaporation accounts for the large core and shallow profile in cluster number distribution compared to the light distribution in M87.

(ii) Evolution produces a radial dependence in the present-day mass spectrum of clusters such that higher mass clusters predominate in the inner regions. The models also indicate an initial radial dependence in the mass spectrum.

(iii) Likelihood ratio tests reject an initial power law in favor of an initial Gaussian but do not rule out the possibility of an initial core in the profile.

(iv) The best-fit model for M87 has an initial population of 7.25×10^3 clusters with projected radius $R < 50\,\mathrm{kpc}$, about 60% more than is currently observed. Roughly 14% of the initial population are now objects of slightly less than $10^5 M_\odot$; dynamical evolution can strongly modify the specific frequency of globular clusters.

(v) Scaling the calculations to fundamental plane elliptical galaxies indicates that cluster evolution in the differing environments qualitatively accounts for the trend in observed population number versus galaxy luminosity. Smaller galaxies tend to have high densities and thus more rapid evolutionary time scales, so their cluster populations tend to diminish more rapidly.

Some of these inferences, especially (iii), may be biased by the lack of detailed data in the inner galaxy. Point source data for $r < 1'$ will lead to stronger constraints on the size of the initial core and a deeper survey will pick up low luminosity objects and further constrain the luminosity function.

ACKNOWLEDGEMENTS

We thank Scott Tremaine for discussion and Bill Harris, Dean McLaughlin and Steve Zepf for providing data. This work was supported in part by NASA award NAGW-2224.

REFERENCES

Binney, J. & Tremaine, S. 1987, Galactic Dynamics, (Princeton: Princeton U. Press)
Blakeslee, J. P. & Tonry, J. L. 1995, ApJ, 442, 579
Brodie, J. 1993, in The Globular Cluster-Galaxy Connection, ASP Conference Series, v. 48, ed G. Smith & J. Brodie, p. 483
Chernoff, D. & Weinberg, M. D. 1990, ApJ, 351, 121
Cohn, H. 1979, ApJ, 234, 1036
Djorgovski, S. D. & Davis, M. 1987, ApJ, 313, 59
Elson, R. & Santiago, B. 1996, MNRAS, 278, 617
Faber, S. M. 1995, private communication
Faber, S. M. & Jackson, R. E. 1976, ApJ, 204, 668
Faber, S. M., Dressler, A., Davies, R. L., Burstein, D., Lynden-Bell, D., Terlevich, R., Wegner, G. 1987, in Nearly Normal Galaxies: From the Planck Time to the Present, ed. S. M. Faber, (New York: Springer-Verlag), p. 175
Freedman, W. L., Madore, B. F., Mould, J. R., Hill, R., Ferrarese, L., Kenicutt, R. C., Saha, A., Stetson, P. B., Graham, J. A., Ford, H., Hoessel, J. G., Huchra, J., Hughes, S. M., Illingworth, G. D. 1994, Nature, 371, 757
Harris, W. E. 1991, ARAA, 29, 543
Harris, W. E. 1996, private communication
Harris, W. E. & Pudritz, R. E. 1994, ApJ, 429, 177
Huchra, J. 1988, in The Harlow-Shapley Symposium on Globular Clusters in Galaxies, ed. J. Grindlay & A. Philip, (Boston: Kluwer), p. 255
Kissler, M., Richtler, T., Held, E. V., Grebel, E. K., Wagner, S. J., Capaccioli, M. 1994, A&A, 287, 463
Lee, H., Fahlman, G., & Richer, H. 1991, ApJ, 366, 455
Lee, M. & Geisler, D. 1993, in The Globular Cluster-Galaxy Connection, ASP Conference Series, v. 48, ed G. Smith & J. Brodie, p. 576
Lauer, T. R. 1988, ApJ, 325, 49
Lauer, T. R. & Kormendy, J. 1986, ApJ, 303, L1
Martin, B. 1971, Statistics for Physicists, (New York: Academic Press)
Mihos, J. C. & Hernquist, L. 1994, ApJ, 437, L47
Murali, C. & Weinberg, M. D. 1996, MNRAS, submitted (MW)
McLaughlin, D. E. 1995, AJ, 109, 2034
McLaughlin, D. E. & Harris, W. E. 1995, private communication
McLaughlin, D. E., Harris, W. E., & Hanes, D. A. 1994, ApJ, 422, 486 (MHH)
McLaughlin, D. E. & Pudritz, R. E. 1996, ApJ, 457, 578
Ostriker, J., Binney, J. & Saha, P. 1989, MNRAS, 241, 849 (OBS)
Ostriker, J. & Tremaine, S. 1975, ApJ, 202, L113
Pahre, M. A., Djorgovski, S. G. and de Carvalho, R. R. 1995, ApJ, 453, L17
Santiago, B. X & Djorgovski, S. G. 1993, MNRAS, 261, 753
Strom, S., Strom, K., Wells, D., Forte, J., Smith., M. & Harris, W. 1981, ApJ, 245
van den Bergh, S. 1995, preprint
van der Marel, R., 1994 MNRAS, 270, 271
Weinberg, M. D. 1994, AJ, 108, 1414
Zepf, S. E., & Ashman, K. M. 1993, MNRAS, 264, 611
Zepf, S. E., Geisler, D. & Ashman, K. M. 1994, ApJ, 435, L117

APPENDIX A: CLUSTER DISTRIBUTION FUNCTIONS

The initial cluster population is represented by joint distributions of the phase space density, $f(E)$ and the mass spectrum $\nu(M, r)$:

$$\psi(M, r, E, J) = \frac{\partial N}{\partial M \partial E \partial J} \propto f(E, r)\nu(M, r), \tag{A1}$$

where $\psi(M, r, E, J)$ is the number of stars per unit mass per unit energy per unit angular momentum at a fixed point in space.

For the initial orbit distribution in coreless models, we generalize the isothermal distribution employed by OBS

$$f(E) = \frac{\rho_0}{(2\pi\sigma_0^2)^{3/2}} e^{-E/\sigma_0^2}, \tag{A2}$$

with $\sigma_0^2 = \eta^{-1} v_0^2$. Note that $\eta^{-1} = \frac{1}{2}$ for the isothermal sphere and $\eta^{-1} = \frac{1}{3}$ for the fiducial model employed by OBS. The background gravitational potential of M87 is taken to be a singular isothermal sphere, $\Phi(r) = v_0^2 \ln r$, independent of the cluster distribution. The space number density of clusters for equation (A2) is then

$$n(r) = \rho_0 r^{-\eta}. \tag{A3}$$

We generalize this profile to include a core:

$$n(r) = \rho_0 (r_c^2 + r^2)^{-\eta/2} \tag{A4}$$

where r_c is the core radius of the system. The isotropic cluster distribution function follows from integral inversion (e.g. Binney & Tremaine 1987).

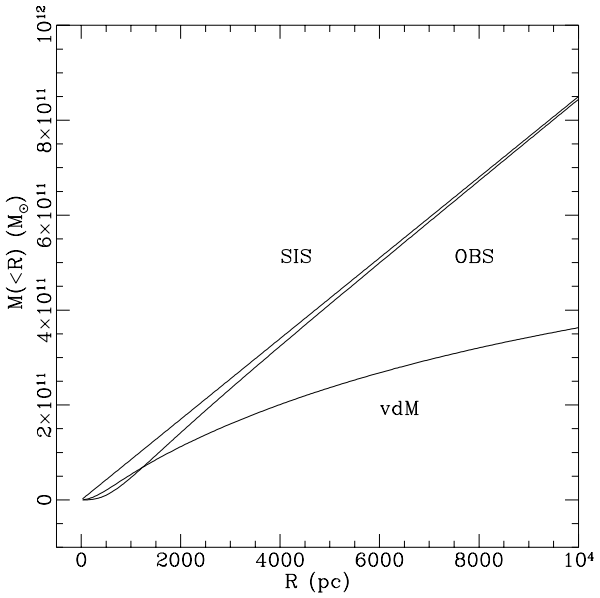

Figure B1. Comparison of singular isothermal sphere (SIS), softened isothermal sphere used by OBS, and the luminosity profile determined by van der Marel (1994). The isothermal models agree with the observed profile at small radii and continue to rise linearly with the dark matter halo.

We consider three initial distributions of cluster masses: 1) a Gaussian distribution of initial magnitudes, V, which is everywhere constant in space (e.g MHH); 2) a power law distribution of mass, M, which is everywhere constant in space (e.g. Harris & Pudritz 1994); and 3) a power law distribution of mass with a radially-dependent spectral index.

The Gaussian distribution of initial magnitudes V defines the mass spectrum

$$\nu(M) \propto e^{-\frac{1}{2}(\frac{V-V_0}{\sigma_V})^2} \frac{dV}{dM}, \tag{A5}$$

where the transformation to mass is effected by the Jacobian, dV/dM. This distribution is characterized by two parameters: V_0 and σ_V, the mean and dispersion of magnitudes.

The simple power law mass distribution

$$\nu(M) \propto M^{-\alpha}, \tag{A6}$$

depends only on the mass spectral index, α. We define the following radially dependent distribution

$$\nu(M, r) \propto M^{-(\alpha + Kr)} \tag{A7}$$

whose spectral index has the central value α and varies linearly with radius.

APPENDIX B: GENERALIZED ISOTHERMAL SPHERE

We adopt a distance of 16 Mpc to M87 which corresponds to $H_0 = 81.5\,\mathrm{km\,s^{-1}\,Mpc^{-1}}$ (van der Marel 1994). This defines a length scale of 77.6 pc per second of arc. Lauer & Kormendy (1986) adopted $H_0 = 75\,\mathrm{km\,s^{-1}\,Mpc^{-1}}$, giving a distance of 17.4 Mpc and defining a length scale of 84.1 pc per second of arc. The more recent estimate by Elson & Santiago (1996) based on the Cepheid calibration of Freedman et al. (1994) gives a length scale of 87 pc per second of arc which is closer to the latter estimate but not strongly discrepant from the first. OBS apparently adopted the length scale of 132 pc per second of arc, corresponding to $H_0 = 50\,\mathrm{km\,s^{-1}\,Mpc^{-1}}$.

For the singular isothermal sphere (SIS), $\Phi(r) = v_0^2 \ln r$, we adopt $v_0 = 606\,\mathrm{km\,s^{-1}}$ (OBS). This defines a velocity dispersion of $\sigma = 350\,\mathrm{km\,s^{-1}}$ for an initial distribution of luminous matter with $\eta^{-1} = \frac{1}{3}$. Figure B1 compares the mass of the SIS with the softened isothermal sphere used by OBS, and van der Marel's (1994) estimate derived using the luminosity profile and dynamical modeling.

The results presented here do not significantly depend on choice of singular or softened potential. The 10% mass difference at 3 kpc leads to 5% faster evolution in the SIS since the dynamical time scale goes as $\rho^{-1/2}$ in tidally-limited clusters. This is well within the 4.7 kpc core radius of the cluster system determined by McLaughlin (1995). Conversely, the tidal field in the the slowly rising core region of the softened model is closer to that in a Keplerian potential which is stronger and so balances the larger mass of the SIS.

APPENDIX C: MAXIMUM LIKELIHOOD ESTIMATION OF MODEL PARAMETERS

A joint χ^2-maximum likelihood estimator is used in §4 to fit the dynamical models to V-band photometric data and binned surface density data of the M87 cluster system (MHH). THe expected surface density profiles are the sum of the dynamically evolved model surface density, $S(r, v; \theta)$, derived from distributions in §3, and background surface density, $\sigma_0(V)$, multiplied by the incompleteness factor, $f(x, y, V)$ which represents the probability of detecting a cluster of given magnitude at a particular location in the field. The likelihood statistic

$$L = \prod_j f(x_j, y_j, V_j) \big[S(r_j, V_j; \theta) + \sigma_0(V_j) \big], \tag{C1}$$

defines the posterior probability of the data given the model. The χ^2 statistic

$$P_{\chi^2} = \prod_i \frac{1}{\sqrt{2\pi}\sigma_i} e^{-\frac{1}{2}\left(\frac{S_i - S(r,\theta)}{\sigma_i}\right)^2}. \tag{C2}$$

defines the posterior probability of the binned data given the model. The total posterior probability is then

$$P = P_{\chi^2} \times L \tag{C3}$$

and the parameters which maximize the posterior probability of the data are the best estimates.